A rubber mount model. Application to automotive equipment suspension

Lionel Manin, Régis Dufour, Benjamin Thomas, Philippe Goge

A rubber mount model. Application to automotive equipment suspension

B. Thomas[1, 2], L. Manin[1,3], Ph. Goge[2], R. Dufour[1]
[1] Université de Lyon, CNRS, INSA-Lyon, LaMCoS UMR5259, F69621, Villeurbanne,
[2] Valeo Engine Cooling, Branch Simulation Department, La Verrière, France

[3] Corresponding author: lionel.manin@insa-lyon.fr

Abstract
In order to predict the nonlinear dynamic response of automotive equipment supported by rubber mounts, it is proposed to extend the generalized Dahl model for taking into account the visco-elastic behaviour of elastomer mount and to combine it, in a next step, with the reduced dynamic equations of the equipment supposed to exhibit a linear behaviour. To this end, the parameters of the restoring force model of the mounts are identified through a series of tests accounting several types of solicitation. The procedure applied to the measured force-deflection loops makes automatic the data processing and thus the parameter identification of the model. The application concerns the suspension of an automotive engine cooling module.

1 Introduction

The qualification of on-board manufactured components forces the automotive suppliers to subject their products to vibration tests defined by standards that are more and more drastic for fitting the complex car environment solicitations. On-board automotive equipments are subjected to base or active excitations which can be time varying, combined, superposed, see Figure 1.

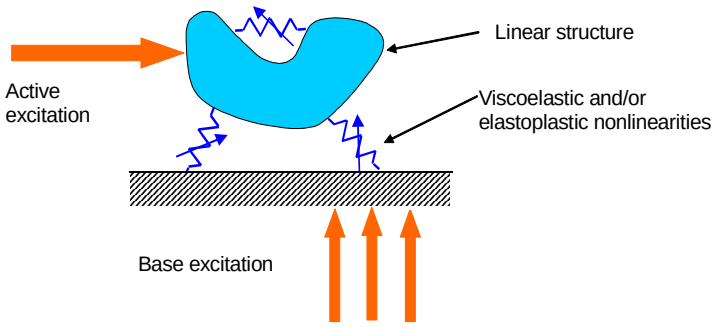

Figure 1: Solicitation environment of linear on-board equipment with nonlinear suspension

Amongst all the different types of suspension, see the review of Ibrahim [1], the passive suspension made of elastomer mounts remains the best choice regarding the economical-performance compromise. For reducing the numbers of tests, it takes advantages to develop a FE model involving the nonlinearities and dissipation brought mainly by the rubber mounts. The dynamic condensation technique associated with the FE method is usually used because it is well-adapted for modeling the linear behavior of structures, Craig and Bampton [2]. The physical degrees of freedom (DOF) kept in the reduced basis permit connecting the nonlinear mechanical component, Gjika and al. [3]. To sum-up modelling rubber mounts requires to take into account a multi-parameter dependence because, pre-load, type of excitation, forcing frequency, frequency and amplitude deflection, warm-up and ambient temperature have different effects on the nonlinear behaviour (Nashif, Jones and Henderson [4]), Petitet, Braquins [5]).

The non linear behavior of mechanical components can be modeled either by parametric models or non-parametric models (Vestroni and Noori [6]). The former provide stiffness and damping parameters (such as Kelvin Voigt, Maxwell, Masing models), that are introduced in the first member of the equation of motion while the latter give a restoring force (such as the Dahl model) introduced in the second member. Al Majid and Dufour proposed a generalized Dahl model for force-deflection loop. It can model different behaviors such as softening, hardening or a combination of both and has been used for predicting the time response of a beam with an all-metal mount, subjected to shocks [8], and to harmonic force [9]. Then it has been applied to belt tensioner (Michon and al.[10]) and passive actuator for the autonomous hexapod deployment. As these previous mechanical components provide elastic and dry-friction forces, they exhibit, at contrary to the rubber mount, an elasto-plastic behavior that is forcing frequency independent. Consequently, modeling rubber mount requires extending the generalized Dahl model for taking into account the visco-elastic effect. This is the purpose of this article.

Section 2 presents the Dahl model generalized by Al Majid and Dufour [8] and its extension to the rubber mount used for the automotive equipment suspension. The experimental tests are carried out on the rubber mounts within their environment, i.e. with the connecting parts to the cooling module. The objective is to demonstrate that this restoring force model is efficient and easy to use and can advantageously replace rheological models. It is described by a first order differential equation which can be coupled with equations of motion of the equipment, forcing the non linear response prediction to be integrated in the time domain. Section 3 presents a data processing permitting the automatic identification of the model parameters by analyzing measured force –deflection loops. The specific interpolation, presented in section 4, gives the model parameters for any force deflection loops in the parameter ranges. Finally the implementation of the generalized Dahl model extended to the rubber mount is implemented in a FE code. Then, experimental and numerical force-deflection loops of rubber mounts used for the suspension of an engine cooling module are compared.

2 Generalized Dahl model extension

The investigated rubber mounts are made of pure elastomer, exhibiting a visco-elastic behaviour. Moreover the equipment-mount interface and the end-stop phenomena add also deflection nonlinearities. Therefore establishing a FE model is not obvious for such a component and it is logical to extract the required parameters from measured force-deflection loops which depends also on temperature, forcing frequency. Such a non linear behavior makes the prediction of the global assembly delicate, (Lacarbonara and Vestroni [7]). In order to obtain the most general and easily formulated model possible, the aim is to model the force deflection loop based on boundary curves, which can be temperature, frequency and amplitude dependent.

2.1 The generalized Dahl's model (GDM)

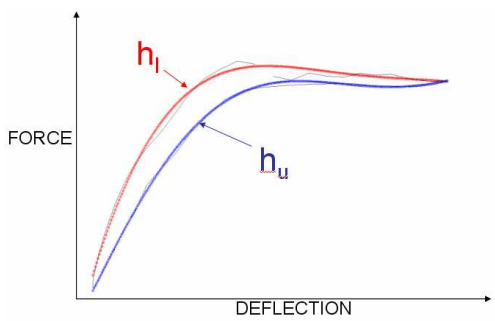

Figure 2: Example of h_u and h_l boundary curves

The GDM, that is a force-deflection model, has been proposed by Al Majid and Dufour ([8], [9]). Let u and R be the deflection and restoring force respectively. The model is expressed as:

$$\frac{dR}{dt} = \beta \frac{du}{dt} * (h - \mathrm{sgn}(\frac{du}{dt}) * R) \tag{1.}$$

where

$$h = 0.5 * ((h_u - h_l) * \mathrm{sgn}(\frac{du}{dt}) + (h_u + h_l)) \tag{2.}$$

with β a parameter that has a stiffness dimension and h_u, h_l the upper and lower boundary curves approximated by a polynomial expansion which can depend on deflection, rate of deflection, temperature, forcing frequency, etc.. Consequently this model can take into account a combination of the environmental effects such as dry friction, visco-elastic behavior, mechanical gaps or end-stops, but requires an experimental investigation for identifying its parameters.

2.2 Experimental identification of the rubber mount

In order to illustrate the procedure for evaluating the GDM parameters, let the experimental identification be carried out on upper and lower rubber mounts, which support an automotive engine cooling module, see Fig. 3.

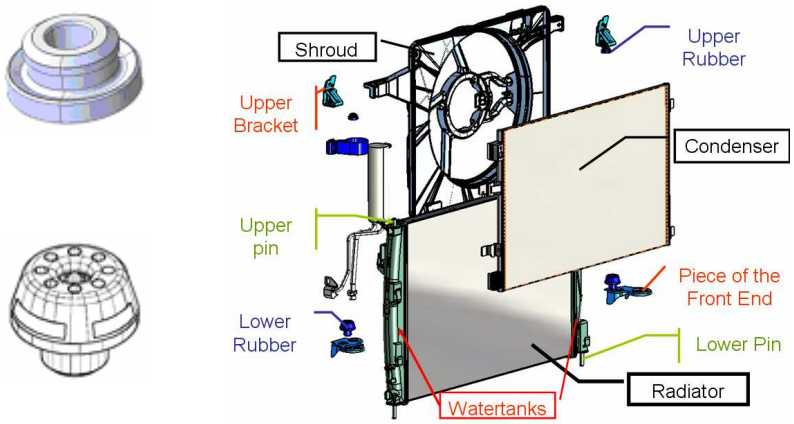

Figure 3: Exploded view of the cooling module

(a) (b) (c)

Figure 4: Testing devices for shear (a) and axial (c) tests applied on the rubber mount equipped of its interfaces.

Two testing apparatus have been designed to test the rubber mounts in traction-compression (see Fig.4a) and in shear deflections, (see Fig. 4c). It should be noted that the transverse test shown in Fig. 4a is performed with two mounts in order to remove the bending effect. A particular attention was paid on the boundary conditions of the rubber mount available in operating condition: these are plastic and metallic interfaces. For the lower rubber mount, the pin of the watertank is used as the exciter connection and a piece of the front end as housing. They enable to keep the gaps and dry friction effects.

An electrodynamic shaker subjected the item to a sinusoidal excitation with a deflection amplitude u_1 controlled by a closed-loop, and a forcing frequency Ω. A bias u_0 permits to impose a preload. The forcing frequency range has been chosen from a real power spectral density (PSD) test. Acceleration recordings gave the range of the deflection, and the maximum frequency is chosen as twice of the frequency range (usual criteria for mode extraction in PSD numerical simulation). The deflection imposed to the rubber is measured by an eddy current sensor, and the transmitted force by a piezo-electric cell load.

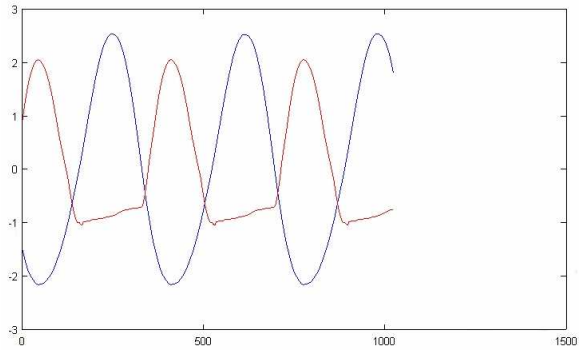

Figure 5: Deflection (blue) and force (red) samples in the time domain

The force and deflection time histories plotted in Fig. 5 highlight that the lower rubbers has a nonlinear behavior, see Fig. 6: designed for supporting a part of the module weight, it has the degree of freedom to translate along the pin of the watertank in the presence of the sinusoidal forcing. Indeed, for large deflections, the rubber mount is no more compressed, and force reaches a threshold, see Fig. 6. Moreover, increasing the forcing deflection amplitude introduces a loop shift due to the lower rubber mounts which leaves more and more the hole in which it is inserted.

Once the measured force-deflection loops are obtained, an automatic data processing has to be established for identifying the GDM parameters.

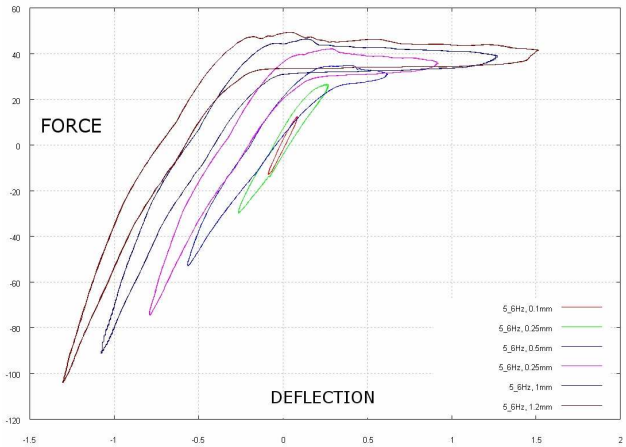

Figure 6: Force-deflection loops recorded at 5.6Hz for different deflection amplitudes

3 Automatic model parameter identification

3.1 Average cycle extraction

The first step of the parameter fitting process is to correct the raw experimental data to make their processing easier and run faster. Indeed, experimental data are often corrupted with noise, it seems better to evaluate an average hysteresis loop from the loops recorded.

Hence, a spatial averaging of the values is performed (Fig. 7). The working plane that contains the cycle is partitioned with small rectangular areas. A sweep is made on all the rectangles to define if points of the curves are present or not in it. Each time several points are surrounded by the rectangle, an average point is created as a barycentre of all the points.

The main advantage of this method is its robustness but it's time consuming. In the version we programmed, blank corners are first removed from the sweeping to gain time on the process.

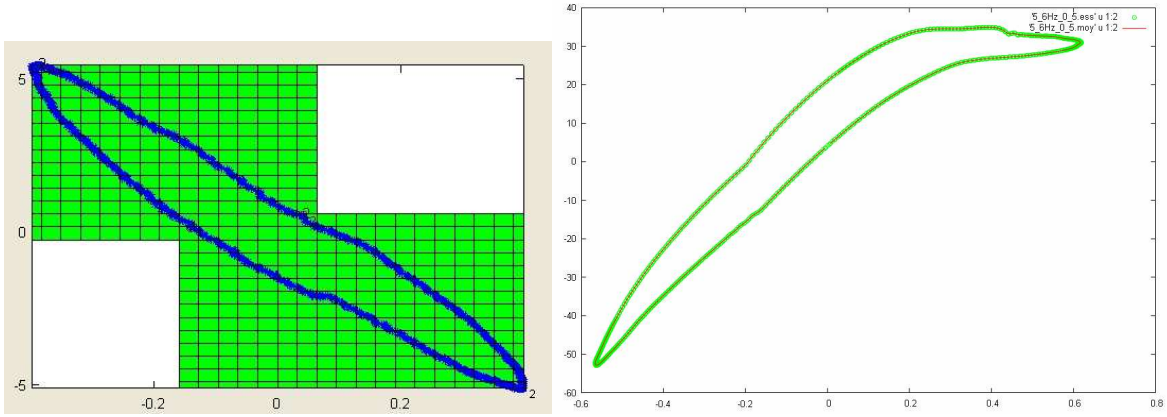

Figure 7: Spatial averaging, example of result average cycle(red), on original points (red)

3.2 Skeleton extraction

After obtaining an average cycle, the scaling of Dahl's model parameters require a sorting of the points. We have to define for each point if it belongs to the upper or the lower curve of the cycle. We decide to automate this sorting by comparing the coordinates of the point to a skeleton curve equation. The points corresponding to the skeleton curve must first be created. We evaluate their coordinates thanks to a sweeping on abscissas. For each abscissa range, a skeleton point is created as an average of the ordinates of the curve points existing in the range. A polynomial interpolation can be used to obtain an approximate equation of the skeleton curve.

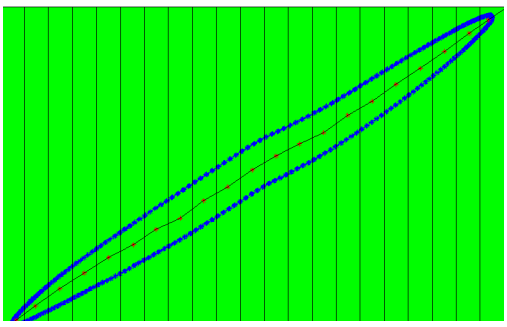

Figure 8: Cycle with its skeleton curve

All point coordinates can then be injected in the skeleton curve equation. The result enables to define if the point is upper or lower than the curve.

3.3 Equivalent excitation

The imposed displacement during the test may not correspond exactly to what is defined in the control software. Therefore, it can be necessary to evaluate what are the real values from the measurements. Since our excitation is harmonic we have to evaluate U_0 and U_1 as:

$$U = U_0 + U_1 \sin(\omega t) \tag{5.}$$

These parameters are obtained by calculating the intersection points of the two polynomial envelop curves. These points correspond to the roots of the function defined by:

$$Q(x) = P_u(x) - P_l(x) \tag{6.}$$

where $P_u(x)$ and $P_l(x)$ are the polynomial functions corresponding to the upper and lower envelops. Actually, the intersection points satisfy the relation:

$$P_u(x) = P_l(x) \tag{7.}$$

In our case study, the polynoms order is larger than 2. Therefore, there can be more than 2 real roots for the function *Q*. We have to eliminate complex roots and non physical values. This method can lead to not consistent results if the 2 polynomials have no intersection point in a reasonable range of displacement, that is why we need to be able to modify manually these parameters.

3.4 β Evaluation – Stokes' theorem

The β parameter is closely linked to the inner area of the hysteretic loop. An automated procedure to evaluate the value of this parameter can be based on the difference between the area of the experimental cycle and the area of the calculated cycle from the identified model parameters.

The area of any surface can be approached thanks to differential geometry. Stokes' theorem [11], which is a central result on differential form integration, enables to obtain formula to switch from perimeter to area.

Stokes Theorem: Let *M* be an oriented smooth manifold of dimension *n* and let w be an *n-1* differential form that is compactly supported on M. So, we have:

$$\int_M dw = \int_{\partial M} w \tag{8.}$$

where *d* denotes the exterior derivative,∂M the boundary of *M*.

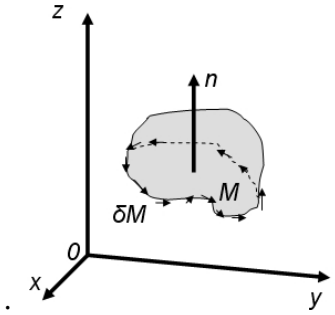

Figure 9: Stokes' theorem illustration

Another version of this theorem known as the Green Riemann theorem [12] gives a differential form on $\Re^2$:

$$\int_{\partial M} [f.dx + g.dy] = \iint_M \left[\frac{\partial g}{\partial x} - \frac{\partial f}{\partial y} \right] dxdy \tag{9.}$$

To obtain immediately an area definition, the best is to define the differential form as:

$$\left(\frac{\partial g}{\partial x}-\frac{\partial f}{\partial y}\right)=2 \quad \text{With g=x and f=-y} \tag{10.}$$

With the previous equation we obtain:

$$\int_{\partial M}\left[-y.dx+x.dy\right]=2\iint_{M}dxdy \tag{11.}$$

or:

$$0.5*\int_{\partial M}\left[-y.dx+x.dy\right]=\iint_{M}dxdy=S \tag{12.}$$

where S is the inner area of the surface. Finally, the discrete formulation is given by:

$$0.5*\sum_{i}^{n}-y_i.dx_i+x_i.dy_i=S \tag{13.}$$

where dx_i et dy_i can be calculated as :

$$\begin{aligned} dx_i &= \left(x_{i+1}-x_{i-1}\right)/2 \\ dy_i &= \left(y_{i+1}-y_{i-1}\right)/2 \end{aligned} \tag{14.}$$

β can then be evaluated by comparison between the experimental area and the model area.

3.5 Iterative reconstruction of the restoring force model

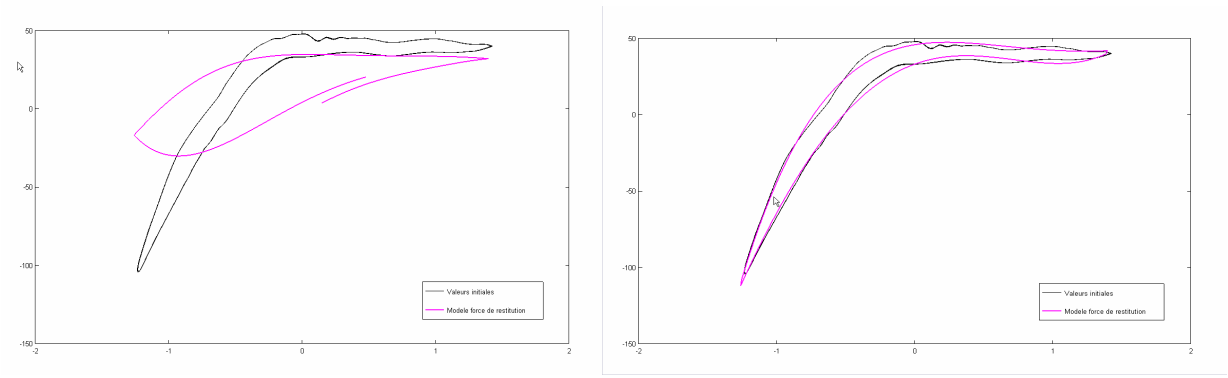

Figure 10: Reconstructed cycles obtained with 3rd order polynomials β = 1 (left), with 3rd order polynomials β = 262 (right)

In our case study, the two envelop curves h_u and h_l are easily approximated thanks to polynomial regression. Several tests enabled to obtain a satisfying fitting of the cycle with 3rd order polynomial forms of the deflection u such as:

$$R=a_0+a_1u+a_2u^2+a_3u^3 \tag{15.}$$

Where the a_n coefficients depend on the excitation parameter. The reconstruction of the restoring force model is based on the incremental calculation of the restoring force thanks to its derivative.

$$R_2=R_1+\frac{dR}{dt}*dt \tag{16.}$$

where $\frac{dR}{dt}$ is given by (1).

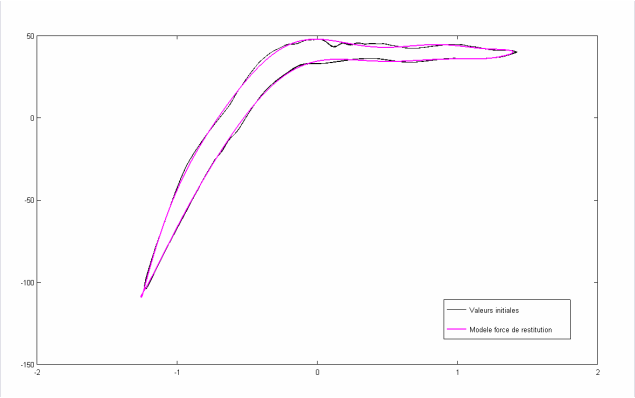

Figure 11: Reconstructed cycle with a 9th order polynomial beta=262

4 Model use – Bilinear Interpolation

It is reminded that the rubber model is established in order to be fully integrated in a global dynamic transient simulation. It means that at each time of the simulation the model should provide a restoring force that corresponds to a frequency and an amplitude of a given deflection. From all the tests performed, we have identified several sets of model parameters corresponding each to one couple (deflection amplitude – frequency) and therefore to one hysteresis loop. The purpose is now to pass from one cycle to another since from two different times the amplitude of deflection and its frequency may change.

4.1 Presentation

Several ways have been investigated to be able to shift from one cycle to another in terms of deflection amplitude and frequency of solicitation. This shift between cycles can be realized through an expression or an interpolation of the polynomial coefficients a_n (see Eq. 15.)

f	5,6	5,6	5,6	5,6	5,6	10	10	10	10	10	18	18	18	18	32	32	32	56	56
u	0,27	0,57	0,81	1,11	1,38	0,27	0,57	0,81	1,11	1,38	0,27	0,57	0,81	1,11	0,27	0,57	0,81	0,27	0,57
a0	7,4839	20,453	32,92	42,574	48,921	7,9862	19,985	32,652	42,236	47,923	8,3573	20,565	33,376	42,314	8,3475	21,762	35,636	8,4313	22,293
a1	117,55	75,395	48,373	26,723	17,777	121,15	73,816	48,725	26,291	15,622	124,86	74,923	50,483	27,237	125,55	75,603	42,903	129,09	72,016
a2	-117,47	-91,341	-80,27	-58,012	-46,648	-123,3	-95,276	-87,378	-63,69	-50,541	-126,24	-101,45	-93,538	-67,044	-118,81	-101,23	-90,68	-129,75	-108,35
a3	-209,23	-8,1804	33,426	28,278	21,595	-225,3	-2,0293	40,284	33,972	26,938	-253,62	-1,3392	43,134	36,159	-208,63	-2,4162	48,135	-246,97	12,743

Figure 12: Table of parameters for several excitations (f frequency, u deflection amplitude)

It can be seen on the above figure that a_n values change in various way depending on excitation parameters. In our case, we consider this evolution only based on the frequency and the amplitude of the excitation. Actually standard automotive supplier vibration tests occur in normal conditions of hygrometry, pressure and temperature. Considering only these two excitation conditions enables to represent the a_n parameters values as 3D surfaces (Fig. 13).

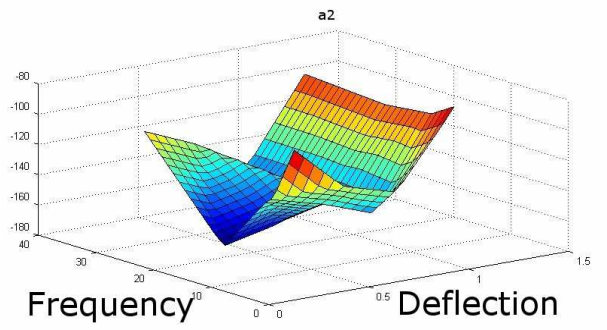

Figure 13: Example of an a_n response surface

The method consists in a bilinear interpolation of the value of the restoring force itself, or of the parameters of the model, i.e the polynomial coefficients.

4.2 Interpolation Principe

We choose here to make a parallel with finite element models. All couples of excitation parameters (deflection, frequency) can be considered as a node of a mesh, numbered by ascending order in deflexion and then in frequency. Each element is a rectangle with four nodes.

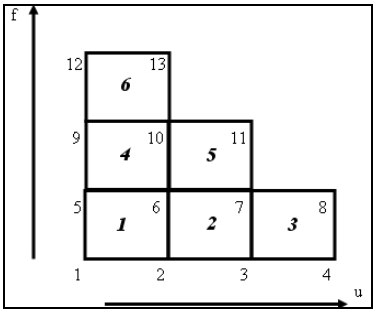

Figure 14: Mesh defined by tests points

As we can see in the figure 14, the test space is often defined as triangle area. Actually, high frequencies of excitation do not enable high amplitude of deflection (due to the shaker limitations). Rectangle elements require that we force excitation couples points to have same frequencies or deflections. That is why we have to define excitation nodes as an average of similar frequencies or displacements. This precision is really important because finite elements interpolation requires geometrical functions to go from real element to perfect shaped element in a reference space [13].

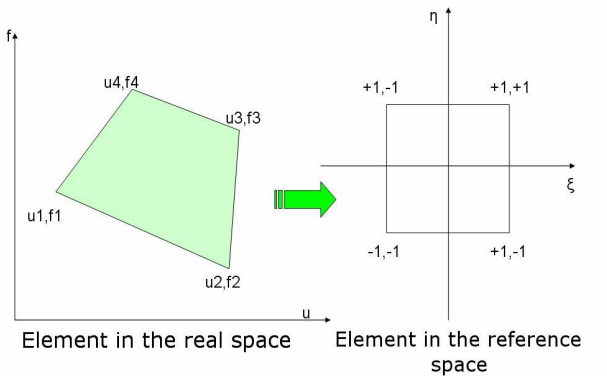

Figure 15: Space changing

The rectangular shape of our elements enables to express easily geometrical functions as:

$$\xi_k(u,f)=\frac{u-\frac{u_k(MAX)+u_k(Min)}{2}}{\frac{u_k(MAX)-u_k(Min)}{2}} \quad \text{and} \quad \eta_k(u,f)=\frac{f-\frac{f_k(MAX)+f_k(Min)}{2}}{\frac{f_k(MAX)-f_k(Min)}{2}} \tag{17.}$$

The evaluation of maximum *u* (displacement) and *f* (frequency) can be automated thanks to the expression of the vectors of the connectivity matrix. Finally, the value to interpolate *A* (corresponding to one of the a_n) can be obtained anywhere in the element thanks to $[A1 \quad A2 \quad A3 \quad A4]$ the value of *A* at each node of the element as:

$$A(u,f)=\left\langle \frac{(1-\xi_k)(1-\eta_k)}{4} \quad \frac{(1+\xi_k)(1-\eta_{k)}}{4} \quad \frac{(1+\xi_k)(1+\eta_k)}{4} \quad \frac{(1-\xi_k)(1+\eta_k)}{4} \right\rangle \begin{Bmatrix} A1 \\ A2 \\ A3 \\ A4 \end{Bmatrix} = N * A_k \tag{18.}$$

The main advantage of this method is its simplicity of implementation once the matrix formulation is defined.

4.3 Out-of-range points

Numerical computations of time displacement and force response can lead to points that do not belong to the test space. That is why it is compulsory to integrate a processing for these points, to prevent solver crashes. It is proposed to consider out of range points belonging to virtual elements which nodes are created as linear dependant to real points insuring continuity.

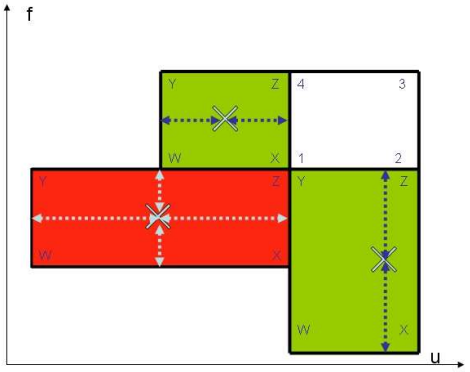

Figure 16: Virtual elements illustration

The virtual element is created so that the out-of-range point is located at the middle of an edge. The value of *A* is given at the virtual nodes considering it is linear regarding the two closer real nodes aligned with the virtual one. For example, for the *Y* node the upper left virtual element of figure 16:

$$A_y=\frac{A_4-A_3}{u_4-u_3}*u_y+(A_4-\frac{A_4-A_3}{u_4-u_3}*u_4) \tag{19.}$$

The same principle is use for corner elements but the calculation is done twice on the last point, once considers the value as linear in term of displacement, once in term of frequency. The retained value is finally an average of the two previous results.

A generalization of the method has been created to enable the reconstruction of an entire surface of response, on the basis of a triangle test surface. In particular, the definition of interaction between real and virtual elements must be carefully analyzed. The results of interaction are shown on figure 17.

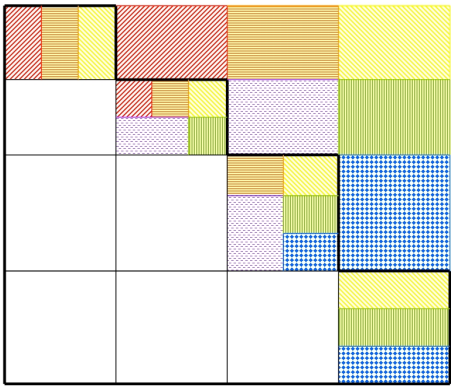

Figure 17: Interaction between real and virtual elements

This method enables to take into account as many data from the real elements as possible to be able to give a plausible response for every non predictable excitation that could occur during the simulation.

The interpolation method results in the implementation of the following data processing algorithm for choosing the good elements of the mesh, or virtual elements that will give the most accurate results.

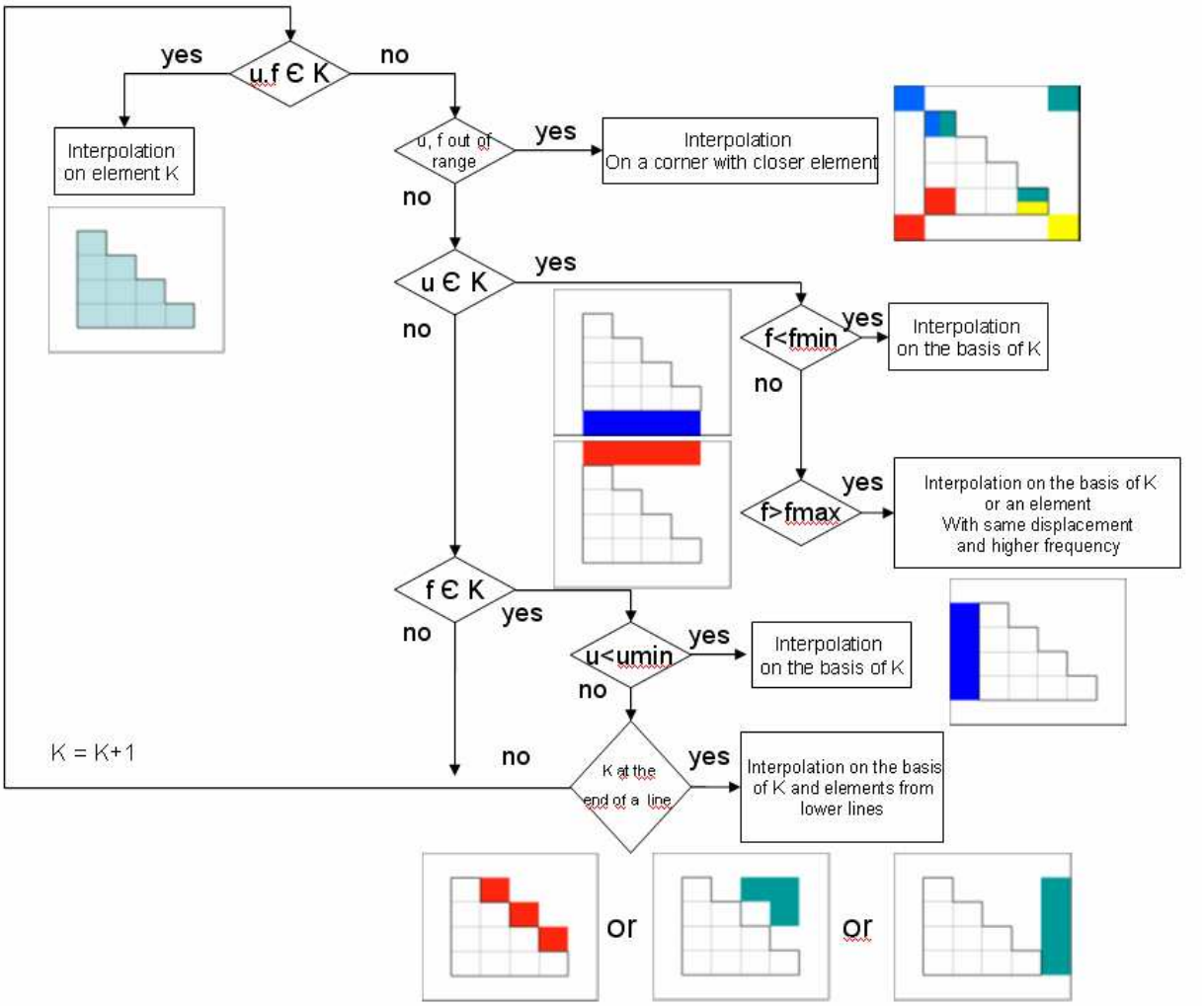

Figure 18: Support element choice algorithm

The process enables to create surfaces of response on the basis of the test mesh.

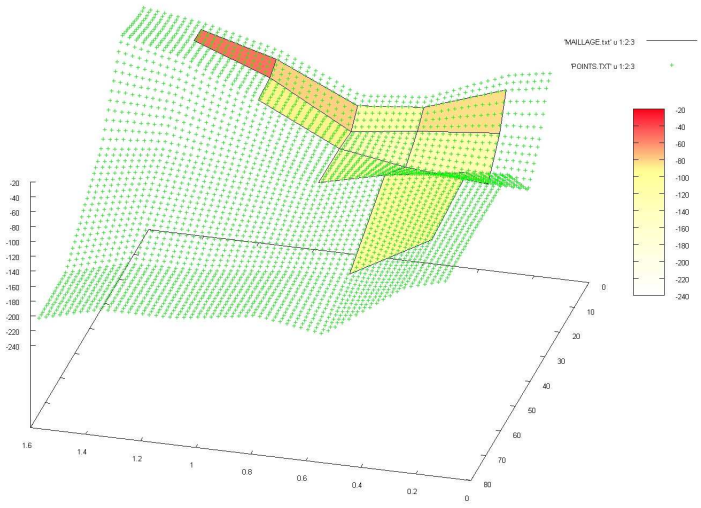

Figure 19: Example of extrapolated surface of response representing the values of a_2

5 Results and solver integration

Automotive suppliers perform random vibration tests on their components within the car manufacturer environment. In the case of engine cooling module, it requires validating the structure with its non linear supporting mounts. Actually, such rubber components are not taken into account in all numerical simulations whereas they can have a big impact on the structure dynamic behavior. The usual average impact appears thanks to the stress criteria value use to validate simulation results. Actually, the numerical stress value defined as critical has been scaled comparing simulation results to failure observed in tests. This empirical solution doesn't enable to have a real fatigue post-processing on the basis of the calculated stress levels.

That's why a numerical model of rubbers, fully integrated to an industrial Finite Element Analysis (FEA) solver, is required.

5.1 Results

The whole process has been programmed on OCTAVE, GNU-licensed MATLAB-like application [1].

The automated data processing is integrated to a program called RUB.I.S. Its interface enables to perform the post processing of tests data with modifiable parameters such as the degree of the polynomial interpolation, the range of force and deflection, the frequency. After uploading a results file, a first processing is performed with a 6^{th} order polynomial form. The user can then modify parameters to better fit the experimental cycle. A report can be saved as a text file to generate a matrix which characterizes the rubber.

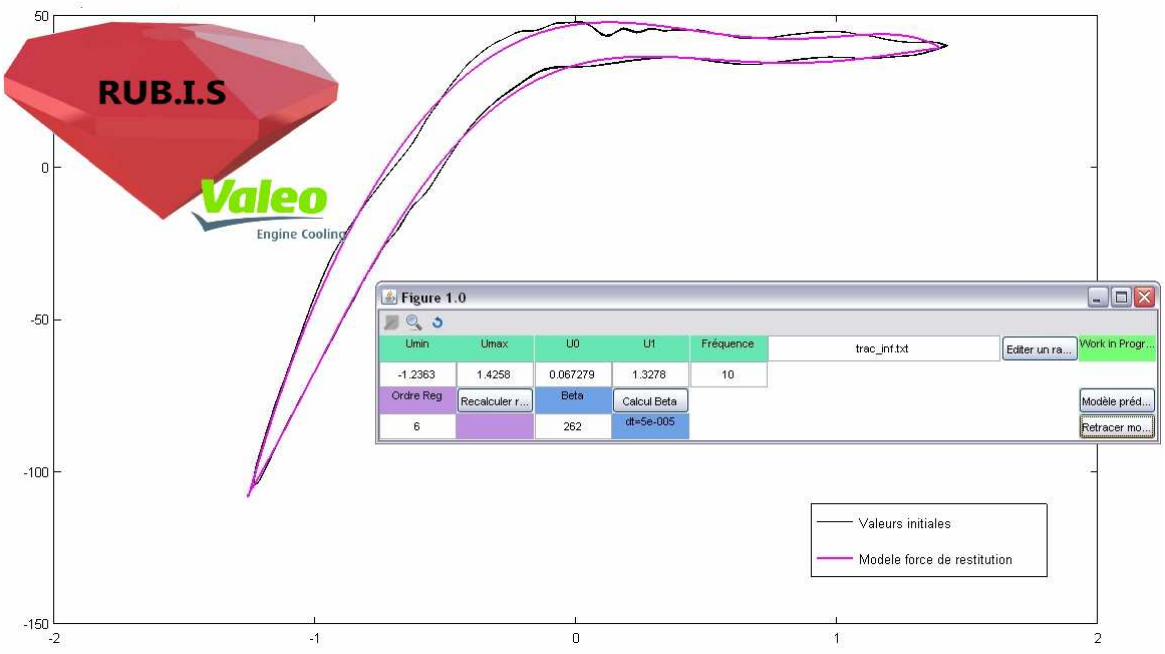

Figure 20: Example of RUB.I.S data processing

RUB.I.S enables to quickly characterize the rubber among a wide range of excitations. A program to generate interpolated hysteric cycles has also been realized an enables to reconstruct measured cycles.

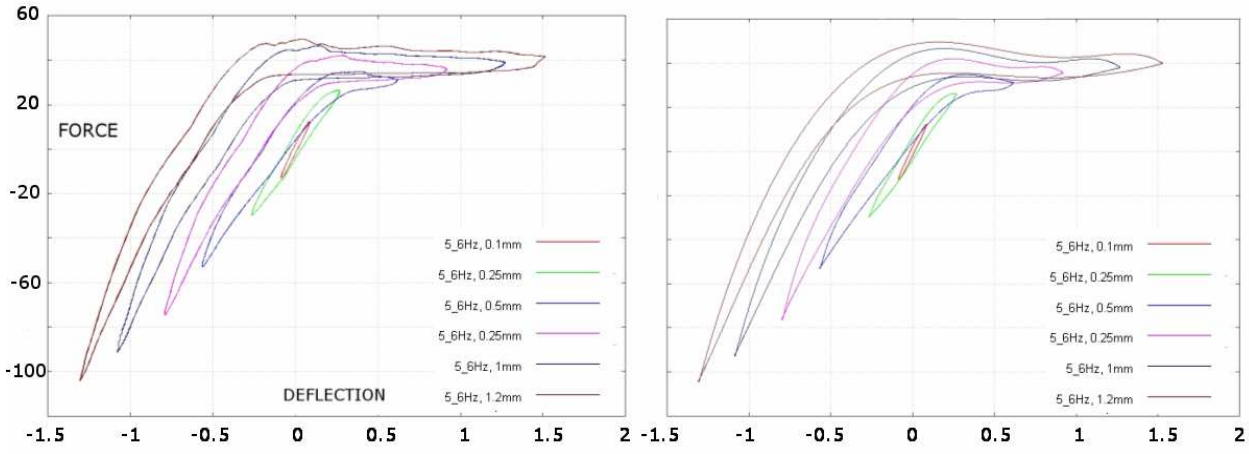

(a) (b)

Figure 21: Comparison between measured (a) and simulated (b) cycles

5.2 Integration to Abaqus

The model and the algorithms developed have been integrated to Abaqus 6.9 thanks to user subroutines. In particular, the routine UAMP enables to define an amplitude value with commands defined by the user. Our amplitude is obtained thanks to previously defined algorithm and interpolation with frequency and displacement obtained from the Finite Element simulation. This amplitude modulates a force imposed at a node representing the upper bound of the rubber. Abaqus Viewer enables to post process history outputs to draw the hysteretic cycles.

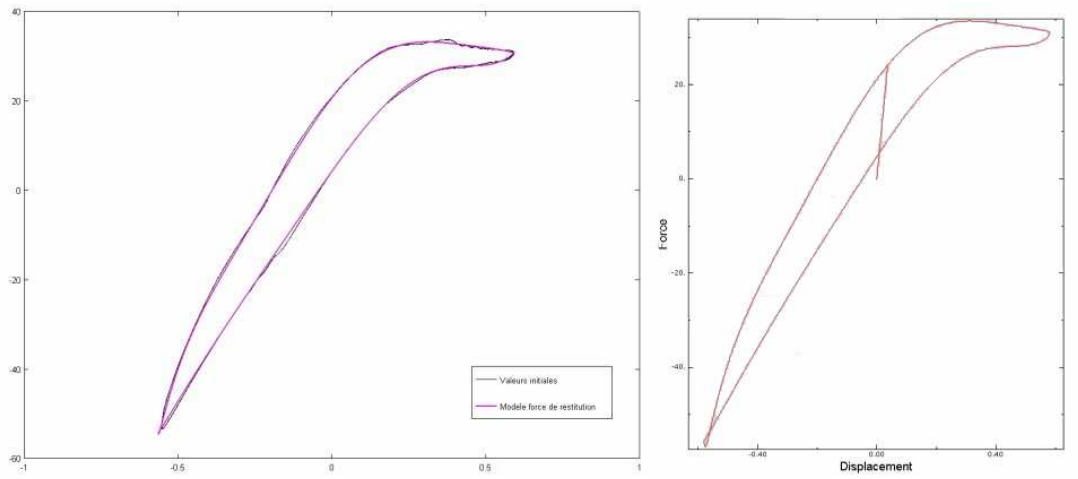

(a) (b)

Figure 22: Comparison between experimental cycle (a) and Abaqus results (b)

The proposed method enables to directly obtain the hysteretic behavior of the rubber with Abaqus.

6 Conclusion

An efficient method to automatically scale the parameters of the modified Dahl's model has been defined. Implemented in an Octave-based software, this method generates the inputs variables of an FEM-like FORTRAN interpolation routine. This routine has been exploited within the industrial solver Abaqus to simulate characteristics hysteresis of the rubbers of an automotive Engine Cooling module.

The next steps of this study consist in the modelling of a real PSD test thanks to temporal simulation and dynamic condensation with Abaqus, first on an academic structure, and then on a complete engine cooling module within its front end.

Acknowledgements

The authors would like to thank Valeo Engine Cooling for its financial and technical support.

References

[1] R.A. Ibrahim, *Review: recent advances in nonlinear passive vibration isolators*, Journal of Sound and Vibration, Vol. 314, Academic Press (2008), pp. 371-452.

[2] R.R. Craig, M.C.C. Bampton, *Coupling of substructures for dynamic analysis*, AIAA Journal, Vol.6(7), 1968

[3] K. Gjika, R. Dufour, G. Ferraris, *Transient response of structures on viscoelastic or elastoplastic mounts: prediction and experiment*, Journal of Sound and Vibration, Vol. 198(3) (1996), Academic Press (pp. 361-378.

[4] D. Nashif, D.I.G Jones. And J.P. Henderson, *Vibration damping*, New York: Wiley (1985)

[5] G. Petitet, M. Barquins, *Matériaux caoutchouteux- Morphologies, Formulations, Adhérence, Glissance et Usure*, Presses Polytechniques Romandes (2008)

[6] F. Vestroni, M. Noori, *Hysteresis in mechanical systems - modelling and dynamic response*, International Journal of Non-Linear Mechanics, Vol. 37, Elsevier Science (2002), pp. 1261–1262

[7] W. Lacarbonara, F. Vestroni., , *Nonclassical responses of oscillators with hysteresis*, Nonlinear Dynamics, Vol.32, Springer Netherlands (2003), pp. 235–258.

[8] A. Al Majid, and R. Dufour., *Formulation of a hysteretic restoring force model. Application to vibration isolation*, Nonlinear Dynamics, Vol. 27, Springer Netherlands (2002),pp. 69-85

[9] A. Al Majid, and R. Dufour, *Harmonic response of a structure mounted on an isolator modelled with a hysteretic operator: experiments and prediction*, Journal of Sound and Vibration, Vol. 277 (1-2), Academic Press (2004), pp. 391-403.

[10] G. Michon,L. Manin, and R. Dufour, *Hysteretic behaviour of a belt tensioner: modelling and experimental investigation*, Journal of Vibration and Control, Vol. 11 (9),Academic Press (2005), pp. 1147-1158

[11] A. Macdonald, *Stokes' Theorem*, Department of Mathematics, Luther College, Decorah U.S.A,(2004)

[12] J.E. Marsden, *Differential Forms and Stokes' Theorem*, Control and Dynamical Systems, Caltech (2006)

[13] J.L. Batoz , G. Dhatt, *Modélisation des structures par éléments finis – Volume 1 Solides Elastiques*, Hermes (1990), pp168-169

[14] J.D. Bonjour, *GNU Octave &Octave Forge –Logiciel libre de calcul numérique, visualisation et programmation,* Ecole Polytechnique Fédérale de Lausanne, Faculté ENAC (2006)